Peer-reviewed version available at *Materials* **2020**, *13*, 3512; doi:10.3390/ma13163512

Negative Effective Mass in Plasmonic Systems, II: Elucidating of Optical and Acoustical Branches of Vibrations and the Possibility of Anti-Resonance Propagation

Edward Bormashenko, Irina Legchenkova, Mark Frenkel

Department of Chemical Engineering, Ariel University, Ariel, Israel 407000

Correspondence: Dr. Edward Bormashenko: E-Mail: edward@ariel.ac.il

Tel.: +972 074 729 68 63

Abstract

We report the negative effective mass metamaterials based on the electro-mechanical coupling exploiting plasma oscillations of a free electron gas. The negative mass appears as a result of vibration of a metallic particle with a frequency of ω which is close to the frequency of the plasma oscillations of the electron gas m_2 relatively to the ionic lattice m_1. The plasma oscillations are represented with the elastic spring $k_2 = \omega_p^2 m_2$, where ω_p is the plasma frequency. Thus, the metallic particle vibrated with the external frequency ω is described by the effective mass $m_{eff} = m_1 + \frac{m_2\omega_p^2}{\omega_p^2-\omega^2}$, which is negative when the frequency ω approaches ω_p from above. The idea is exemplified with two conducting metals, namely Au and Li embedded into various matrices. The one-dimensional lattice built of the identical metallic micro-elements m_{eff} connected by ideal springs k_1 representing various media such as polydimethylsiloxane and soda-lime glass is treated. The optical and acoustical branches of longitudinal modes propagating through the lattice are elucidated for various ratios $\frac{\omega_1}{\omega_p}$. The 1D lattice built of the thin metallic wires giving rise to the low frequency plasmons is treated. The possibility of the anti-resonant propagation, strengthening the effect of the negative mass occurring under $\omega = \omega_p = \omega_1$ is addressed.

Keywords: metamaterials; negative effective mass; plasma oscillations; low frequency plasmons; optical and acoustical branches.

Introduction

Metamaterials are artificial materials demonstrating properties that is not found in naturally occurring materials [1-3]. In metamaterials the index of refraction and magnetic permittivity may be negative at certain frequencies. Moreover, they may be tuned in a broad range of values [4]. One of the most rapidly developed fields within the domain of metamaterials is the field of photonic band-gap crystals, which are multidimensional periodic structures with a period

Peer-reviewed version available at Materials 2020, 13, 3512; doi:10.3390/ma13163512

of the order of the optical wavelength [5-7]. The theory predicted the existence of a photonic bandgap (PBG), a frequency band of inhibited optical modes [5-6]. Analogously, acoustical band gap materials were predicted and manufactured [8-11]. In particular sonic crystals, based on the idea of localized resonant structures, that exhibit spectral gaps with a lattice constant two orders of magnitude smaller than the relevant wavelength were reported [10-11].

Acoustic metamaterials, in which both the effective density and bulk modulus are simultaneously negative, in the true and strict sense of an effective medium have been reported [12]. Acoustic metamaterials demonstrating the negative Poisson's ratio [13] and negative elastic modulus were discussed [14]. Mechanical metamaterial exhibiting auxetic behavior and negative compressibility were suggested [15]. Acoustic metamaterials demonstrate a potential as perfect absorbers of mechanical vibrations [16] and also as materials enabling focusing of ultrasound [17]. In our recent paper we proposed to exploit the plasma oscillations of the electron gas for the development of the metamaterials with the negative effective mass (density) [18]. The notion of the negative effective mass (density) acoustic metamaterials was introduced in Refs. 19-21. We suggested to exploit the so-called plasma oscillations of the electron gas [22] for the development of the metamaterials with the negative effective mass (density) [18]. Now we elucidate the structure of the optical and acoustical branches of elastic waves propagating in chain structures built of elements possessing the negative effective mass, exploiting the plasma oscillations in metal particles connected by ideal springs, representing elastic media.

1. Results and discussion

1.1. Propagation of harmonic waves in the 1D lattice comprising negative effective mass plasmonic elements

The mechanical model giving rise to the negative effective mass effect, introduced in refs. 20, 21, 23 is depicted in **Figure 1**. A core with mass m_2 is connected internally through the spring with k_2 to a shell with mass m_1. The system is exerted by the external sinusoidal force $F = \hat{F} sin\omega t$. If we solve the equations of motion for the masses m_1 and m_2 and replace the entire system with a single effective mass m_{eff} we obtain [20, 21, 23]:

$$m_{eff} = m_1 + \frac{m_2\omega_0^2}{\omega_0^2-\omega^2} \quad , \tag{1}$$

where $\omega_0 = \sqrt{\frac{k_2}{m_2}}$. It is easily recognized that when the frequency ω approaches ω_0 from above the effective mass m_{eff} will be negative [20, 21, 23]. In our recent paper we suggested the electro-mechanical, plasmonic analogy of the aforementioned model, giving rise to the negative effective

Peer-reviewed version available at Materials 2020, 13, 3512; doi:10.3390/ma13163512

mass [18]. Consider a cubic metal particle shown in **Figure 1A**, seen as atomic lattice m_1 containing the Drude-Lorenz free electrons gas possessing the total mass of $m_2 = m_e nV$, where $m_e = 9.1 \times 10^{-31}$kg is the mass of electron, n is the concentration (number density) of the electron gas and V is the volume of the particle [22, 24, 25]. Electron gas is free to oscillate with the plasma frequency $\omega_p = \sqrt{\frac{ne^2}{m_e \varepsilon_0}}$ [22, 24, 25]. Expose the entire metal particle to the external sinusoidal force $F = \hat{F} sin\omega t$. The effective mechanical scheme of the metallic particle is shown in **Figure 1B** and it exactly coincides with that giving rise to the negative effective mass, supplied in this case by:

$$m_{eff} = m_1 + \frac{m_2 \omega_p^2}{\omega_p^2 - \omega^2} \quad , \tag{2}$$

where m_1 is the mass of the ionic lattice, m_2 is the total mass of the electron gas; it is seen that it may be negative when the frequency ω approaches ω_p from above [18]. It was demonstrated that the effective dimensionless mass $\frac{m_{eff}}{m_1 + m_2} \cong \frac{m_{eff}}{m_1}$ is independent on the metallic particles' size [18]. The results of calculations of the effective negative mass for Li and Au are supplied in Ref. 18 (the physical parameters of these metals are summarized in **Table 1**).

Consider now the one-dimensional lattice built of elements (cells) shown in **Figure 1B** and depicted in **Figure 2.** The 1D lattice is built of identical elements possessing the effective negative masses m_{eff} given by Eq. 2 and connected by ideal springs k_1; the separation between the elements a is constant, as shown in **Figure 2**. Consider propagation of harmonic wave (ω, q):

$$u_i^{k+n}(x,t) = \hat{u}_0 e^{j(qx + nqa - \omega t)}, \tag{3}$$

where $u_i^{k+n}(x,t)$ is the displacement of the mass i $(i = 1,2)$ in the $k+n$-cell, $\hat{u}_0$ is the complex wave amplitude, q is the wave number [21]. The dispersion equation for the 1D lattice depicted in **Figure 2** was derived in Ref. 21:

$$m_1 m_2 \, \omega^4 - \left[(m_1 + m_2)k_2 + 2m_2 k_1 \big(1 - cos(qa)\big)\right]\omega^2 + 2k_1 k_2 \big(1 - cos(qa)\big) = 0 \tag{4}$$

Dividing Eq. 4 by $m_1 m_2$ and considering $\frac{m_1}{m_2} \gg 1$ (which is true for plasmonic systems, thus, we can neglect m_2 in the sum $m_1 + m_2$) and $k_2 = m_2 \omega_p^2$ yields Eq. 5:

$$\omega^4 - \left[\omega_p^2 + 2\frac{k_1}{m_1}\big(1 - cos(qa)\big)\right]\omega^2 + 2\frac{k_1}{m_1}\omega_p^2 [1 - cos(qa)] = 0 \tag{5}$$

Denoting $\omega_1^2 = \frac{k_1}{m_1}$ supplies in turn:

$$\omega^4 - \left[\omega_p^2 + 2\omega_1^2 \big(1 - cos(qa)\big)\right]\omega^2 + 2\omega_1^2 \omega_p^2 [1 - cos(qa)] = 0 \tag{6}$$

Peer-reviewed version available at *Materials* **2020**, *13*, 3512; doi:10.3390/ma13163512

Equation 6 yields following exact solutions:

$$\omega = \omega_p \tag{7.1}$$

$$\omega = \omega_1\sqrt{2\left(1 - cos(qa)\right)} = 2\omega_1 \sin\frac{qa}{2} \tag{7.2}$$

The solution of Eq. 6 gives rise to the "acoustic" and "optical" branches of vibrations [26, 27]. The solution supplied by Eq. 7.1 inherent for plasma oscillations of the electron gas corresponds to the absence of dispersion within the optical branch of vibrations; whereas, the solution supplied by Eq. 7.2 corresponds to the well-known dispersion inherent for propagation of longitudinal acoustic waves propagating within homogeneous 1D lattice, possessing the lattice constant of a [27]. In the limiting case of $qa \to 0$ we obtain the non-dispersion propagation $\omega = \omega_1 qa$ corresponding to the continuous string, possessing the highest eigenfrequency of $\omega = \omega_1$.

The degenerated double-resonance propagation occurs when $\omega = \omega_p = \omega_1$ takes place. This propagation corresponds to the so-called antiresonance, when the amplitude of vibration of the mass m_1 is minimal and in the limiting case even equals zero [28-29]. When the antiresonance $\omega = \omega_p = \omega_1$ condition is fulfilled all of the energy is transferred to the mass m_2, thus strengthening the effect of the negative mass.

"Optical" and "acoustical" branches of longitudinal modes propagation in the 1D lattice, depicted in **Figure 2** for various $\frac{\omega_1}{\omega_p}$ ratios are shown in **Figures 3A-C** [26-27]. It is recognized from **Figure 3**, that the relative location and configuration of the optical and acoustical branches depends strongly on the ratio $\frac{\omega_1}{\omega_p}$. The optical and acoustical branches may be separated by the frequency (energy) gap, as shown in **Figure 3A**. The configurations of optical and acoustical branches at which this gap is zero are also possible, as shown in **Figures 3B**, **C**. It is noteworthy that the optical and acoustical branches may intersect, as depicted in **Figure 3C**.

In order to exemplify the suggested meta-material, we considered the 1D lattice of spherical Li and Au particles, dispersed in the polymer (polydimethylsiloxane) and soda-lime glass matrices. The values of the spring stiffness [30] and frequencies ω_1 calculated for various diameters of the metallic particles ($D \cong 10^{-7} - 10^{-6}\, m$) and lattice constants ($a \cong 1.5 \times 10^{-7} - 1.5 \times 10^{-6}\, m$) are summarized in **Table 2**. It is clearly recognized from the numerical data supplied in **Tables 1, 2**, that for the suggested composite meta-materials the interrelation $\omega_p >> \omega_1$ takes place. Thus, the relative location of the acoustic and optical branches of modes, resulting in the formation of the band gap, depicted in **Figure 3A**, necessarily occurs.

Peer-reviewed version available at Materials 2020, 13, 3512; doi:10.3390/ma13163512

Exemplification of the situations presented in **Figures 3B, C** demands an essential decrease in the plasma frequency, which is possible in the meta-materials, addressed in the following section.

1.2. Propagation of harmonic waves in the metallic meso-structures demonstrating the effect of negative effective mass.

The plasma oscillations shown in **Figure 1** will demonstrate the negative mass in the vicinity of the plasma frequency which is on the order of magnitude of $\omega_p \cong 10^{16}\text{Hz}$, which is very high. However, this frequency may be strongly decreased for the meso-structures built of thin metallic wires, as demonstrated in Ref. 31. Depression of the plasma frequency into the far infrared and even GHz band becomes possible due to the mutual inductance appearing in the periodic arrays built of thin metallic wires arranged in a simple cubic lattice, joined at the corners of the lattice [31], such as depicted in **Figure 4**. Consider longitudinal acoustic modes propagating along such a lattice. For a sake of simplification, we replace the 3D lattice with the 1D lattice, shown in **Figure 2**. The effective (pseudo) density of electrons in the metamaterial lattice shown in **Figure 4** is given by [31]:

$$\tilde{n} \cong \pi n \frac{r^2}{l^2}, \tag{8}$$

where l is the lattice constant, r is the radius of the wire, n is the concentration of the free electron gas supplied in **Table 1** for Li and Au. The pseudo-mass of electrons in such matrices is given by [31]:

$$\tilde{m} = \frac{\mu_0 r^2 e^2 n}{2} ln \frac{l}{r} . \tag{9}$$

The value expressed by Eq. 9 is called in Ref. 31 as the "effective mass"; however, in our paper the notion of the "effective mass" is already ascribed to the mass of the vibrated element, given by Eq. 1. Thus, we call the value expressed by Eq. 9 the "pseudo-mass", and the effective density of electrons expressed by Eq. 8 we label as the "pseudo-density". Assuming $r = 1.0 \times 10^{-6}\text{m}; l = 5.0 \times 10^{-3}\text{m}$ enables calculation of the effective pseudo-plasma frequencies ω_p^* for Au and Li according to Eq. 10 (Ref. 31):

$$\omega_p^* = \sqrt{\frac{\tilde{n}e^2}{\varepsilon_0 \tilde{m}}} = \sqrt{\frac{2\pi c_0^2}{l^2 \ln(l/r)}}, \tag{9}$$

where $c_0 \cong 3.0 \times 10^8 \frac{\text{m}}{\text{s}}$ is the speed of light in vacuum. Substituting aforementioned numerical parameters yields for the effective plasma frequencies of the lattices built from Au and Li wires $\omega_p^{*Au} = \omega_p^{*Li} = 8.2\ \text{GHz}$, which are already comparable with the frequencies attainable by the modern piezoelectric devices [32-33].

Peer-reviewed version available at *Materials* **2020**, *13*, 3512; doi:10.3390/ma13163512

The relative location of the optical and acoustical branches of the longitudinal modes' propagation in the 1D meta-lattice, depicted in **Figure 4** is similar to that shown in **Figure 3**. However, contrastingly to the situation addressed in the previous section the interrelation $\omega_p \cong \omega_1$ becomes attainable under the reasonable choice of the geometrical parameters l and r. Thus, the anti-resonant propagation, strengthening the effect of the negative mass under $\omega = \omega_p = \omega_1$ becomes possible [28-29].

Again, the configurations of the optical and acoustic branches separated and non-separated by the frequency (energy) gap are possible, as illustrated in **Figure 3**. It should be emphasized that the ensembles of metallic wires, shown schematically in **Figure 4**, will not demonstrate simultaneously the negative mass (density) and the negative refraction effects [34]. This is due to the fact that the negative refraction becomes possible below the plasma frequency ω_p [34]; contrastingly, the effect of the negative mass in our model emerges when the frequency ω approaches ω_p from above; thus, creating of the material, demonstrating simultaneously the negative density and dielectric constant remains challenging.

Conclusions

We address propagation of harmonic longitudinal acoustic waves through the 1D lattice demonstrating the effect of the negative mass arising from the plasma oscillations of the electron gas relatively to the atomic lattice. The effect takes place when a metallic particle is vibrated with the external frequency ω approaching the plasma frequency $\omega_p = \sqrt{\frac{ne^2}{m_e\varepsilon_0}}$ from above. In this case the effective mass of the metallic particle $m_{eff} = m_1 + \frac{m_2\omega_p^2}{\omega_p^2-\omega^2}$, where m_1 is the mass of the ionic lattice, and m_2 is the mass of the electron gas, becomes negative [12, 13, 15, 18, 21]. The plasma oscillations may be phenomenologically represented with the ideal spring $k_2 = \omega_p^2 m_2$. The one-dimensional lattice built of the identical metallic (say Li and Au) elements m_{eff} connected by the ideal springs k_1 enabling electro-mechanical coupling is addressed. Model meta-materials built of Li and Au micro-particles embedded into polymer and glass matrices, represented by ideal springs k_1 are considered. Exact dispersion relations in the case of $\frac{m_1}{m_2} \gg 1$ are elucidated.

The configurations of the optical and acoustical branches of the longitudinal modes propagating through the 1D lattice arising from the various ratios $\frac{\omega_1}{\omega_p}$ are explored [26-27]. The relative location and configuration of the optical and acoustical branches depends strongly on the

Peer-reviewed version available at *Materials* **2020**, *13*, 3512; doi:10.3390/ma13163512

ratio $\frac{\omega_1}{\omega_p}$. The optical and acoustical branches may be separated by the frequency (energy) gap. The possibility of the antiresonant wave propagation arising when $\omega = \omega_p = \omega_1 = \sqrt{\frac{k_1}{m_1}}$ is treated.

The effects due to the negative effective mass become possible in the nearest vicinity of the plasma frequencies, inherent for typical metals which are high, namely $\omega_p \sim 10^{16}$Hz. The plasma frequency may be decreased markedly for the low frequency plasmons predicted for the metallic mesostructures [31], enabling manufacturing metamaterials, demonstrating the negative effective density. The configurations of the optical and acoustic branches separated and non-separated by the frequency (energy) gap are possible. Again, the anti-resonant propagation, strengthening the effect of the negative mass under $\omega = \omega_p = \omega_1$ is feasible [28-29].

Acknowledgements:

The authors are indebted to Mrs. Yelena Bormashenko for her kind help in preparing this work.

Funding:

No external funding was obtained for this work.

References

1. Felbacq, D.; Bouchitté, G. *Metamaterials Modelling and Design*, Taylor & Francis, Pan Stanford Publishing, Singapore, 2017.

2. Engheta, N.; Ziolkowski, R. W. *Electromagnetic Metamaterials: Physics and Engineering Explorations*, IEEE Press, Hoes Lane, NJ, USA, 2006.

3. Kshetrimayum, R. S. A Brief Intro to Metamaterials. *IEEE Potentials*. **2004**, *23* (5), 44–46.

4. Boardman, A. D.; Grimalsky, V.V.; Kivshar, Y. S.; Koshevaya, S. V.; Lapine, M.; Litchinitser, N. M.; Malnev, V. N.; Noginov, M,; Rapoport, Y. G.; Shalaev, V. M. Active and tunable metamaterials. *Laser & Photonics Reviews* **2011**, *5* (2), 287-307.

5. Joannopoulos, J. D.; Villeneuve, P. R.; Fan, S. Photonic crystals. *Solid State Comm*. **1997**, *102* (2–3), 165-173.

6. Joannopoulos, J.; Villeneuve, P.; Fan, S. Photonic crystals: putting a new twist on light. *Nature* **1997**, *386*, 143–149.

Peer-reviewed version available at Materials 2020, 13, 3512; doi:10.3390/ma13163512

7. Baba, T. Slow light in photonic crystals. Nature Photon. **2008**, *2*, 465–473.

8. Kushwaha, M. S., Halevi, P., Dobrzynski, L.; & Djafari-Rouhani, B. Acoustic band structure of periodic elastic composites. *Phys. Rev. Lett*. **1993**, *71*, 2022–2025.

9. Maldovan, M. Phonon wave interference and thermal bandgap materials. *Nature Mater* **2015**, *14*, 667–674.

10. Sheng, P.; Zhang, X. X.; Liu, Z.; Chan, C. T. Locally resonant sonic materials. *Physica B* **2003**, *338* (1–4), 201-205.

11. Liu, Zh.; Zhang, X.; Mao, Y.; Zhu, Y. Y.; Yang, Z.; Chan, C. T.; Sheng, P. Locally resonant sonic materials. *Science* **2000**, *289* (5485), 1734-1736.

12. Li, J.; Chan, C. T. Double-negative acoustic metamaterial. *Phys. Rev. E* **2004**, *70*, 055602(R).

13. Al Sabouni-Zawadzka, A.; Gilewski, W. Smart metamaterial based on the simplex tensegrity pattern. *Materials* **2018**, *11*(5), 673.

14. Chen H.; Ding Ch. Simulated and experimental research of multi-band acoustic metamaterial with a single resonant structure. *Materials* **2019**, *12* (21), 3469.

15. Grima-Cornish, J. N.; Grima, J. N.; Attard, D. A Novel mechanical metamaterial exhibiting auxetic behavior and negative compressibility. *Materials* **2020**, *13*(1), 79.

16. Mei, J.; Ma, G.; Yang, M.; Yang, Zh.; Wen, W.; Shen, P. Dark acoustic metamaterials as super absorbers for low-frequency sound. *Nature Comm*. **2012**, *3*, 756.

17. Zhang, S.; Yin, L.; Fang, N. Focusing ultrasound with an acoustic metamaterial network. *Phys. Rev. Lett*. **2009,** *102*, 194301.

18. Bormashenko, Ed.; Legchenkova, I. Negative effective mass in plasmonic systems. *Materials* **2020**, *13* (8), 1890.

19. Yang, Z.; Mei, J.; Yang, M.; Chan, N. H.; Sheng, P Membrane-type acoustic metamaterial with negative dynamic mass. *Phys. Rev. Lett*. **2008**, *101*, 204301.

20. Chan, C. T.; Li, J.; Fung, K. H. On extending the concept of double negativity to acoustic waves. *JZUS A* **2006,** *7*, 24-28.

21. Huang, H. H.; Sun, C. T.; Huang, G. L. On the negative effective mass density in acoustic metamaterials. *Int. J. Eng. Sci*. **2009**, *47*, 610-617.

Peer-reviewed version available at *Materials* **2020**, *13*, 3512; doi:10.3390/ma13163512

22. Tonks, L; Langmuir, I. Oscillations in ionized gases. *Phys. Rev*. **1929**, *33* (8), 195–210.

23. Huang, Y. Y.; Sun, C. T. Wave attenuation mechanism in an acoustic metamaterial with negative effective mass density. *New J. Phys*. **2009**, *11*, 013003.

24. Mizutani, U. *Introduction to the Electron Theory of Metals*, Cambridge University Press, Campridge, UK, 2001.

25. Ashcroft, N.; Mermin, N. D. *Solid State Physics*, NY, USA, Holt, Rinehart & Winston, 1976.

26. Kittel, Ch. *Introduction to Solid State Physics*, 5th Ed. Wiley, NY, USA, 1976.

27. Harrison, W. A. *Solid State Theory*, Dover Publications Inc., NY, USA, 1980.

28. Wahl, F.; Schmidt, G.; Forrai, L. On the significance of antiresonance frequencies in experimental structural analysis. *J. Sound & Vibration* **1999**, *219* (3), 379-394.

29. Belbasi, S., Foulaadvand, M.E., Joe, Y.S.: Anti-resonance in a one-dimensional chain of driven coupled oscillators. *Am. J. Phys*. **2014**, *82*, 32–38.

30. CRC Handbook of Chemistry and Physics, 92 Edition, Editor-in-Chief: W. M. Haynes, CRC, Boca Rayton, Fl. 2011, USa.

31. Pendry, B.; Holden, A. J.; Stewart, W. J.; Youngs, I. Extremely low frequency plasmons in metallic mesostructures. *Phys. Rev. Lett*. **1996**, *76*, 4773.

32. Liu, Zh.; Zhang, X.; Mao, Y.; Zhu, Y. Y.; Yang, Zh.; Chan, C. T.; Sheng, P.; Ambrosy A.; Holdik, K. Piezoelectric PVDF films as ultrasonic transducers. *J. Phys. E* **1984**, *17*, 856-859.

33. Odagawa, H.; Yamanouchi, K. 10 GHz range extremely low-loss surface acoustic wave filter. *Electronics Lett.* **1998**, *34* (9), 865-866.

34. Veselago, V.; Braginsky, L.; Shklover, V.; Hafner, C. Negative refractive index materials. *J. Comput. Theor. Nanosci*. **2006**, *3* (2), 189-218.

Peer-reviewed version available at *Materials* **2020**, *13*, 3512; doi:10.3390/ma13163512

Table 1. Properties of metals used in the calculations

Metal	ρ, kg/m^3	n_e, m^{-3}	ω_p, Hz
Li	530	4.7×10^{28}	1.0×10^{16}
Au	19300	5.9×10^{28}	1.3×10^{16}

Table 2. Dimensions of spherical metallic particles and physical properties of the matrix materials used in the calculations.

	D, m	a, m	m_1, kg	m_2, kg	k_1, N/m (PDMS)	k_1, N/m (glass)	k_2, N/m (plasma)	ω_1, Hz (PDMS)	ω_1, Hz (glass)
Au	1×10^{-6}	1.5×10^{-6}	1.01×10^{-14}	2.81×10^{-20}	1.18	1.1×10^{5}	3.65×10^{-4}	1.72×10^{6}	5.25×10^{8}
Li	1×10^{-6}	1.5×10^{-6}	2.77×10^{-16}	2.24×10^{-20}	1.18	1.1×10^{5}	2.24×10^{-4}	1.04×10^{7}	3.17×10^{9}
Au	5×10^{-7}	7.5×10^{-7}	1.26×10^{-15}	3.51×10^{-21}	0.59	5.5×10^{4}	4.57×10^{-5}	3.44×10^{6}	1.05×10^{9}
Li	5×10^{-7}	7.5×10^{-7}	3.46×10^{-17}	2.80×10^{-21}	0.59	5.5×10^{4}	2.80×10^{-5}	2.08×10^{7}	6.34×10^{9}
Au	1×10^{-7}	1.5×10^{-7}	1.01×10^{-17}	2.81×10^{-23}	0.12	1.1×10^{4}	3.65×10^{-7}	1.72×10^{7}	5.25×10^{9}
Li	1×10^{-7}	1.5×10^{-7}	2.77×10^{-19}	2.24×10^{-23}	0.12	1.1×10^{4}	2.24×10^{-7}	1.04×10^{8}	3.2×10^{10}

D –diameter of the spherical metallic particle (see **Figure 2**)

a - lattice constant.

Peer-reviewed version available at *Materials* **2020**, *13*, 3512; doi:10.3390/ma13163512

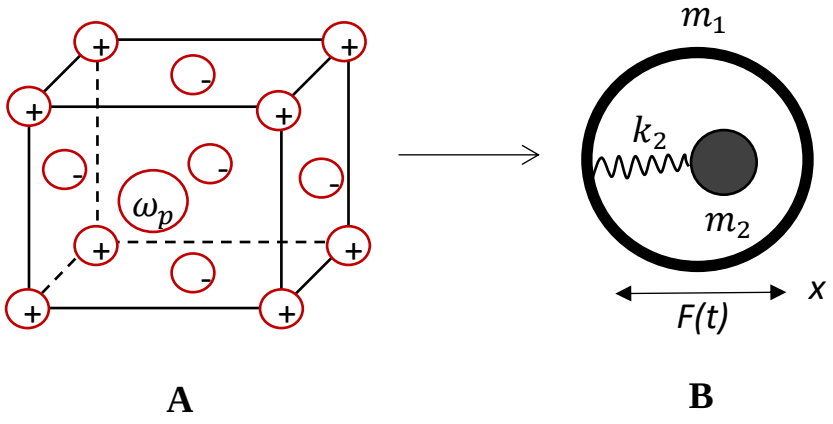

Figure 1. A. Free electrons gas is embedded into the ionic lattice; ω_p is the electron plasma frequency. **B.** The equivalent mechanical scheme of the system **A**. Core with mass m_2 (free electrons gas mass) is connected internally through the spring with $k_2 = \omega_p^2 m_2$ to a shell with mass m_1(ionic lattice mass). The system is subjected to the sinusoidal force $F(t) = \hat{F} sin\omega t$.

Peer-reviewed version available at *Materials* **2020**, *13*, 3512; doi:10.3390/ma13163512

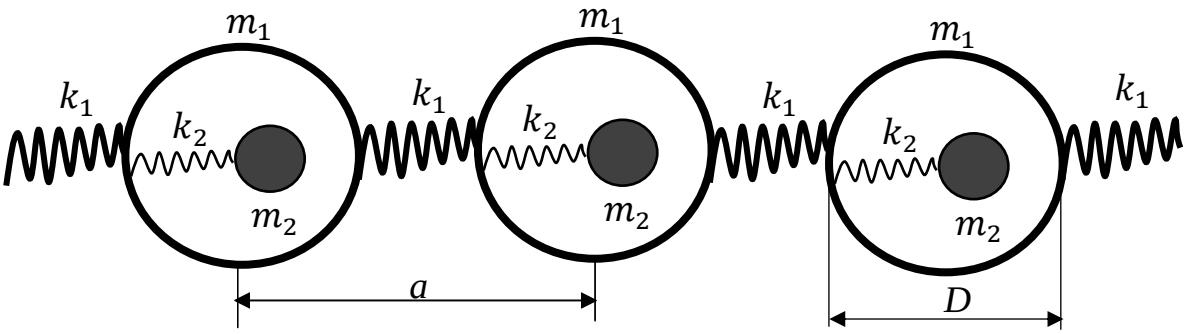

Figure 2. The mechanical scheme of the one-dimensional lattice is depicted.

Peer-reviewed version available at *Materials* **2020**, *13*, 3512; doi:10.3390/ma13163512

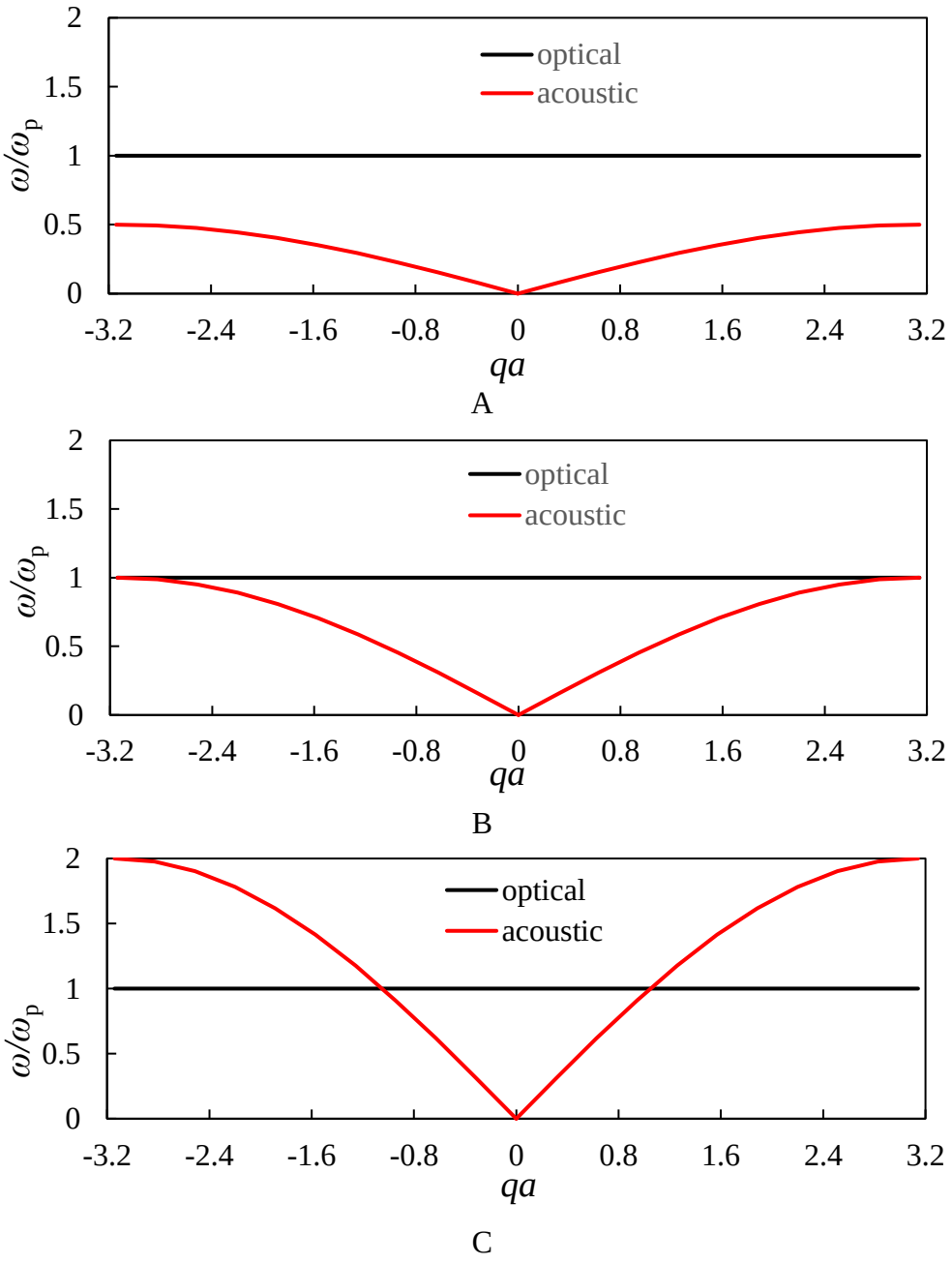

Figure 3. Optical and acoustic branches of longitudinal modes calculated for different ratios $\frac{\omega_1}{\omega_p}$.

A. $\frac{\omega_1}{\omega_p} = 0.25$; **B**. $\frac{\omega_1}{\omega_p} = 0.5$; **C**. $\frac{\omega_1}{\omega_p} = 1$.

Peer-reviewed version available at *Materials* **2020**, *13*, 3512; doi:10.3390/ma13163512

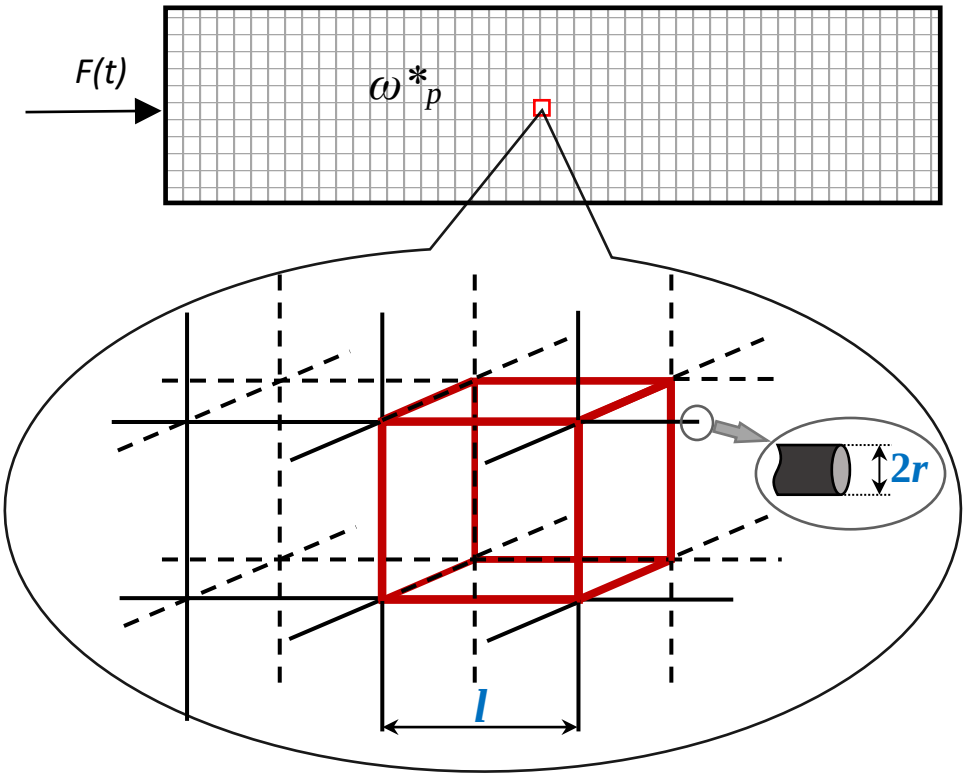

Figure 4. Metallic wires with the radius of r arranged in a simple cubic lattice with the lattice constant of l. The lattice is subjected to the axial sinusoidal force $F(t) = \hat{F} sin\omega t$.